Original Article

JCBFM

Journal of Cerebral Blood Flow & Metabolism
2017, Vol. 37(4) 1264–1275

DOI: 10.1177/0271678X16654157
journals.sagepub.com/home/jcbfm
SAGE

Vascular permeability in the RG2 glioma model can be mediated by macropinocytosis and be independent of the opening of the tight junction

Karin Pernet-Gallay[1,2], Pierre-Henri Jouneau[3,4], Anne Bertrand[1,2], Julie Delaroche[1,2], Régine Farion[1,2], Chantal Rémy[1,2] and Emmanuel L Barbier[1,2]

Abstract

This study evaluates the extravasation pathways of circulating macromolecules in a rat glioma model (RG2) which was observed by both magnetic resonance imaging using ultrasmall superparamagnetic iron oxide and electron microscopy. Although magnetic resonance imaging signal enhancement was observed as soon as 10 min after injection (9.4% 2 h after injection), electron microscopy showed that endothelial cells were still tightly sealed. However, circulating immunoglobulin G and ultrasmall superparamagnetic iron oxide were found in large membrane compartments of endothelial cells, in the basal lamina (7.4 ± 1.2 gold particles/μm^2 in the tumor versus 0.38 ± 0.17 in healthy tissue, $p = 1.4.10^{-5}$) and between tumoral cells. Altogether, this strongly suggests an active transport mediated by macropinocytosis. To challenge this transport mechanism, additional rats were treated with amiloride, an inhibitor of macropinocytosis, leading to a reduction of membrane protrusions (66%) and of macropinosomes. Amiloride however also opened tumoral tight junctions allowing a larger extravasation of ultrasmall superparamagnetic iron oxide (magnetic resonance imaging signal enhancement of 35.7% 2 h after injection). Altogether, these results suggest that ultrasmall superparamagnetic iron oxide and immunoglobulin G in the RG2 glioma model follow an active extravasation pathway mediated by a macropinocytosis process. Amiloride also appears as a potential strategy to facilitate the extravasation of chemotherapeutic drugs in glioma.

Keywords

Neurooncology, blood–brain barrier, microscopy, magnetic resonance imaging, imaging

Received 14 January 2016; Revised 12 April 2016; Accepted 8 May 2016

Introduction

It is well known that the permeability of cerebral blood vessels, the blood–brain barrier (BBB), increases in malignant tumors. This feature, a hallmark of angiogenesis, is routinely used in clinics for diagnosis and therapeutic follow-up. Recently, it has been shown that antiangiogenic drugs (e.g. Sorafenib or Bevacizumab) can close the blood–tumor barrier (BTB) whereas radiotherapy induces an alteration of the BTB in the tissue that surrounds the tumor.[1,2] This alteration of BBB, routinely used as imaging biomarker to assess tumor aggressiveness, can also be an opportunity to facilitate drug delivery. Assessing the

[1]INSERM, U 1216, Grenoble, France
[2]Univ. Grenoble Alpes, Grenoble Institut des Neurosciences, GIN, Grenoble, France
[3]CEA, Institut Nanosciences et Cryogénie, Grenoble, France
[4]Univ. Grenoble Alpes, Institut Nanosciences et Cryogénie, Grenoble, France

Corresponding author:
Emmanuel L Barbier, U1216 – Grenoble Institut des Neurosciences, Chemin Fortuné Ferrini, BP 217—CHU Grenoble, F-38043 Grenoble cedex, France.
Email: emmanuel.barbier@univ-grenoble-alpes.fr

underlying pathways of BBB permeability may concern several brain pathologies.[3]

The permeability of the healthy BBB to a molecule depends on numerous features such as the weight, the charge, and the lipophilicity of the molecule.[4] In a glioma, there is an increase in angiogenic activity due in part to the transcription of the cytokine vascular endothelial growth factor A (VEGF-A) which stimulates endothelial proliferation via the activation of vascular endothelial growth factor receptor 2 (VEGFR-2) tyrosine kinase receptor.[5] VEGF-A has not only a role in activating mitosis and migration of endothelial cells but is also a powerful vascular permeabilizing agent, acting at concentration below 1 nM.[6,7] The permeability of this BTB is, however, less well characterized than that of the BBB.

In the literature, there is debate on the pathways that plasma proteins and other circulating nanomolecules follow when extravasating from vessels in brain tumors. The BBB is structurally composed of four main units: the tight junctions (TJ) between endothelial cells, which prevent the passive diffusion of hydrophilic molecules above 500 kDa; the basal lamina; the pericytes which cover 22–32% of the endothelium; and the astrocytic endfeet which ensure the transport of nutrients from the blood to the neurons.[8] In addition, the BBB is characterized by an absence of endothelial fenestration and a low level of transcytosis.[9] Three main hypotheses have been proposed to explain the increased BBB permeability in tumors: an opening of the TJ,[10,11] an increase in transport across endothelial cells,[12] and the formation of vesiculo-vacuolar organelles that cross endothelial cells.[13]

To better understand how a nanomolecule reaches a brain tumor, we investigated the BTB permeability to 30 nm iron oxide particles and to circulating immunoglobulin G (IgG) which are 11 nm wide. In this study, we used the RG2 rat model of glioma, known to be permeable to iron oxide particles.[14] The microvessel morphology was characterized by electron microscopy (EM) and the BTB permeability was assessed in vivo by magnetic resonance imaging (MRI) using iron oxide particles as contrast agent and postmortem by EM using immunogold labeling to detect endogenous IgG and energy-dispersive X-ray (EDX) spectroscopy to detect the iron oxide particles. As a transendothelial transport through macropinocytosis was observed in our results, rats were submitted to amiloride, a drug known to reduce this type of active cellular uptake.[15]

Material and methods

The study design was approved by the "Grenoble – Institute of Neuroscience" ethics committee for animal care and use (agreement no. 004). Experiments were performed under permits (no. 380820 for CR and A3851610008 for experimental and animal care facility) from the French Ministry of Agriculture. This study is in compliance with the ARRIVE guidelines (Animal Research: Reporting in Vivo Experiments).[16] Male Sprague-Dawley rats ($n = 16$; age = 7 weeks) were obtained from Charles River, France, and housed by groups of 3–4 in Plexiglas cages under standard laboratory conditions (12 h light/dark cycle with lights off at 7:00 p.m. and at a controlled temperature of $22 \pm 2^{\circ}$C). Water and standard laboratory chow were provided ad libitum.

Animals

Experiments were performed on Fischer rats in which RG2 glioma cells were implanted in the striatum using a stereotaxic head holder. RG2 cells were obtained in October 2008 from the American Type Culture Collection (Manassas, VA; ATCC-CRL-2433, Lot number 3618623), tested for infectious diseases in March 2009 (Charles River Animal Diagnostic Service, Wilmington, MA, USA; all negative results) and used in June 2009 (Ampoule passage: 20). Using a Hamilton syringe, a 5 µl cell suspension (5×10^3 RG2 cells) in serum-free cell culture medium was injected over 5 min.

Two groups of rats were considered: one group received amiloride (150 µg/ml of amiloride (Sigma-Aldrich, Saint-Louis, USA) in drinking water (ad libitum) during three days) and one received no treatment. Animals were randomly allocated to each group with the constraint of obtaining similar mean tumor size across each group. Fifteen days after the tumor implantation, rats were imaged by MRI (nonblinded to the group) (cf. below) and sacrificed immediately after.

MRI

Fifteen days after tumor cells injection, MRI was performed as follows. Experiments were done at 4.7 T on a Bruker Avance 3 console using volume/surface cross coil configuration (Bruker Biospin, Germany; MRI facility of Grenoble, IRMaGe). All MRI experiments were performed under anesthesia: 5% isoflurane for induction and 2% for maintenance in air. Rats were maintained at $37.0 \pm 0.5^{\circ}$C throughout the experiments. After anesthesia, the tail vein was equipped with a catheter to deliver contrast agent. The following MRI sequences were then realized:

1. Anatomical T1-weighted images were acquired using a spin-echo MRI sequence (TR/TE = 1000/7.1 ms, NA = 2, 19 slices with FOV $40 \times 40\,mm^2$, matrix = 256×256 and voxel size = $157 \times 157 \times 1000\,\mu m^3$). Acquisition duration was 3 min and 44 s.

2. T1-weighted images were acquired using a spin-echo MRI sequence (TR/TE = 800/5.2 ms, NA = 4, matrix = 128×96 and voxel size $234 \times 234 \times 1000\,\mu m^3$, acquisition of one scan was 1 min 16 s). After the acquisition of four images, ultrasmall superparamagnetic iron oxide (USPIO) were injected in the tail vein of the animal (200 µmol of iron/kg; Sinerem®, Guerbet SA, France) and flushed with a bolus of saline. These USPIO contain an iron core (4–6 nm diameter) surrounded by a dextran shell (~30 nm diameter).[17] Acquisition duration was 90 min.
3. The previously described anatomical T1-weighted sequence was repeated.

The entire MRI session lasted about 2 h for each animal. Immediately after MRI, rats were sacrificed and the tumor tissue was dissected. No necrosis was observed during the dissection process.

Morphological study

The tumor and the normal neuronal tissue from the three rats used in MRI were dissected and cut in 1 mm^3 pieces before being quickly immersed in fixative (2% PFA and 2% glutaraldehyde in 0.1 M cacodylate buffer pH 7.2) during 2 h. Samples were then embedded in an epoxy resin. For this purpose, samples were washed, postfixed with 1% osmium tetroxide in cacodylate buffer, stained in 1% uranyl acetate in water pH 4 during 1 h in the dark, and dehydrated through graded ethanol series before being embedded in epoxy resin (Sigma-Aldrich, St. Louis, USA) that was polymerized during three days at 60°C. Ultrathin sections of the sample (60 nm) were cut with an ultra-microtome (Leica ultracut). Sections were then stained in uranyl acetate and lead citrate before being viewed under a transmission electron microscope at 80 kV (JEOL 1200EX). Images were taken (blinded to the group) at 12,000 and 50,000 magnifications with a digital camera (Veleta, Olympus) and morphometric measurements were done with iTEM software (Soft Imaging System). Experiments were performed at the Electron Microscopy facility of Grenoble, MEC.

Immunogold labeling

Tissue samples of two of the rats used in MRI were fixed with 2% PFA and 0.2% glutaraldehyde in phosphate buffer during 2 h, cryoprotected in 2.3 M sucrose, and frozen in liquid nitrogen on pin sample holder. Ultrathin sections of the frozen samples were obtained with an ultra-cryo-microtome at −120°C. Sections were retrieved with a 1/1 solution of methylcellulose (2%)/sucrose (2.3 M). Immunogold labeling was performed as previously described[18] using 10 nm protein A-gold (CMC, Utrecht).

Scanning EM and analysis

For scanning EM, samples collected at the end of the MRI session from two animals were fixed in 2% PFA, 2% glutaraldehyde in phosphate buffer overnight. Samples were then prepared for cryosections as described above. This cryomethod avoids all dehydration steps that would displace the nanoparticles and does not require heavy metal staining that would mask the nanoparticles which have not a heavy contrast by themselves.

At room temperature, sections were fixed with 1% glutaraldehyde in PBS, washed in distilled water, and stained with 0.5% uranyl acetate in methylcellulose during 10 min. Sections were viewed with a scanning electron microscope (Hitachi 5500) by using the bright field in scanning transmission electron microscopy (STEM) mode at 40 kV. In addition, spectra of the particles were obtained from user-defined areas with the EDX detector, which allows the unambiguous identification of the iron nanoparticles injected in the rats. Experiments were conducted at the nanocharacterization facility of Minatec (CEA-Grenoble).

Histology

Frozen brain tissue from three additional rats was cut with a cryostat (slice thickness = 10 µm). After fixing in methanol/acetone (50% v/v) and washing in tap water for 5 min, one slice was used to highlight cell nuclei, using 4′,6′-diamidino-2-phenylindole (DAPI), and one to highlight vessels, using type IV collagen (against basal lamina). Slices were rehydrated in phosphate-buffered saline (PBS, 0.01 M) and fixed in 4% paraformaldehyde. After saturation in PBS-Tween 0.01%–BSA 3% for 30 min at room temperature, a goat antibody against collagen IV (Southern Biotech, Birmingham, AL, ref. 1340-01, 1/2000) was incubated overnight at 4°C in PBS-Tween 0.01%–BSA 1%. Revelation used an Alexa 546-linked Donkey anti-goat IgG (Invitrogen, Cergy Pontoise, France, ref. A11030, 1/200).

Statistics

All results are expressed as mean ± SEM. The nonparametric Kruskal–Wallis with post hoc Dunn's tests for multiple comparisons or the nonparametric Mann–Whitney tests were used. No data were rejected during analysis. A p value of 0.05 was considered significant.

Results

Capillaries morphology is modified in the tumor but TJs are intact

From a histological point of view, the RG2 glioma was characterized by a high cell density and abnormal microvessels (larger caliber and lower density) if compared to the contralateral tissue (Figure 1). At the ultrastructural level, modifications of the morphology of the blood vessels were not only observed in the tumor but also in the contralateral tissue. Indeed, astrocytic endfeet that normally cover the whole cerebral capillary wall were dilated and formed edema around 35 of the 45 blood vessels observed in the contralateral, nontumor tissue (Figure 1(c)), whereas such modifications were never observed in healthy rats. Inside the tumor, astrocytes were not in contact with the capillaries (Figure 1(f)).

The basal lamina also showed morphological modifications. Blood vessel in nontumoral tissue had a regular thickness of 81 ± 3 nm (134 blood vessels obtained from three rats) whereas in the tumor, the basal lamina surrounding the capillary was thicker (278 ± 18 nm, 119 blood vessels obtained from three rats; $p < 0.0001$) and disorganized (Figure 2). All observed tumor blood vessels had a basal lamina which occasionally became larger than 300 nm (Figure 2(c) to (e)) and, in such occasion, the basal lamina seemed less dense.

No morphological evidence could explain the increase in permeability of the tumor blood vessels: fenestrations were never observed in the endothelial cells and these cells were all linked by TJ with a normal length: 781 ± 66 nm in control (53 TJ obtained from three rats), 976 ± 79 nm in tumor (66 TJ obtained from three rats; $p = 0.06$) (Figure 2(b) and (c)). However, we could observe in the tumor a large

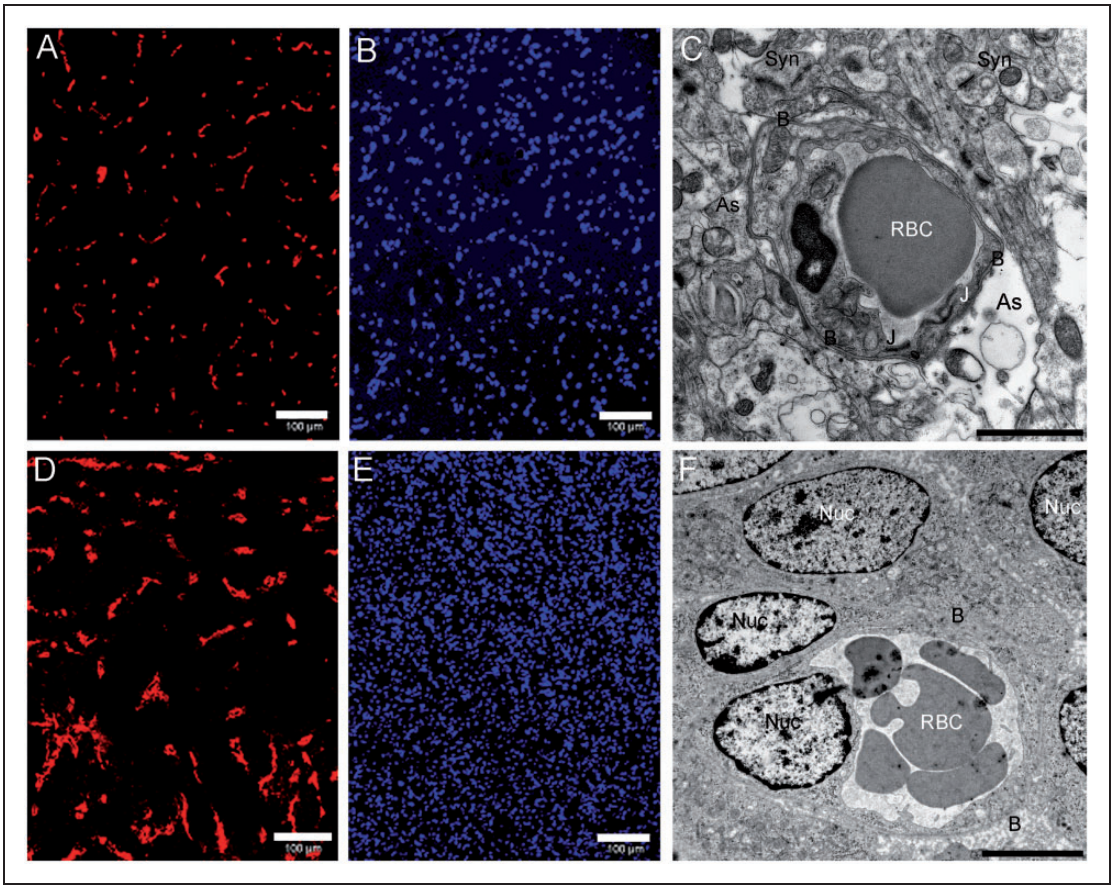

Figure 1. Histological features. (a) Collagen IV staining of contralateral tissue. (b) Nucleus staining (DAPI) of contralateral tissue (bar: 100 μm). (c) Contralateral (nontumoral) tissue imaged by TEM. Synapses are visible (Syn) as well as astrocytic processes (As) which contact the basal lamina (B) that surrounds the capillary. An astrocytic edema is visible at the bottom right (bar: 200 nm). (d) Collagen IV staining of an active tumor area. A larger vascular bed is visible. (e) Nucleus staining (DAPI) of an active tumor area. A higher nucleus density is visible. (f) Tumoral tissue imaged by TEM. Numerous nuclei of tumor cells are visible (Nuc) and the cells directly contact the basal lamina (bar: 200 nm). DAPI: 4',6-diamidino-2-phenylindole; TEM: transmission electron microscopy.

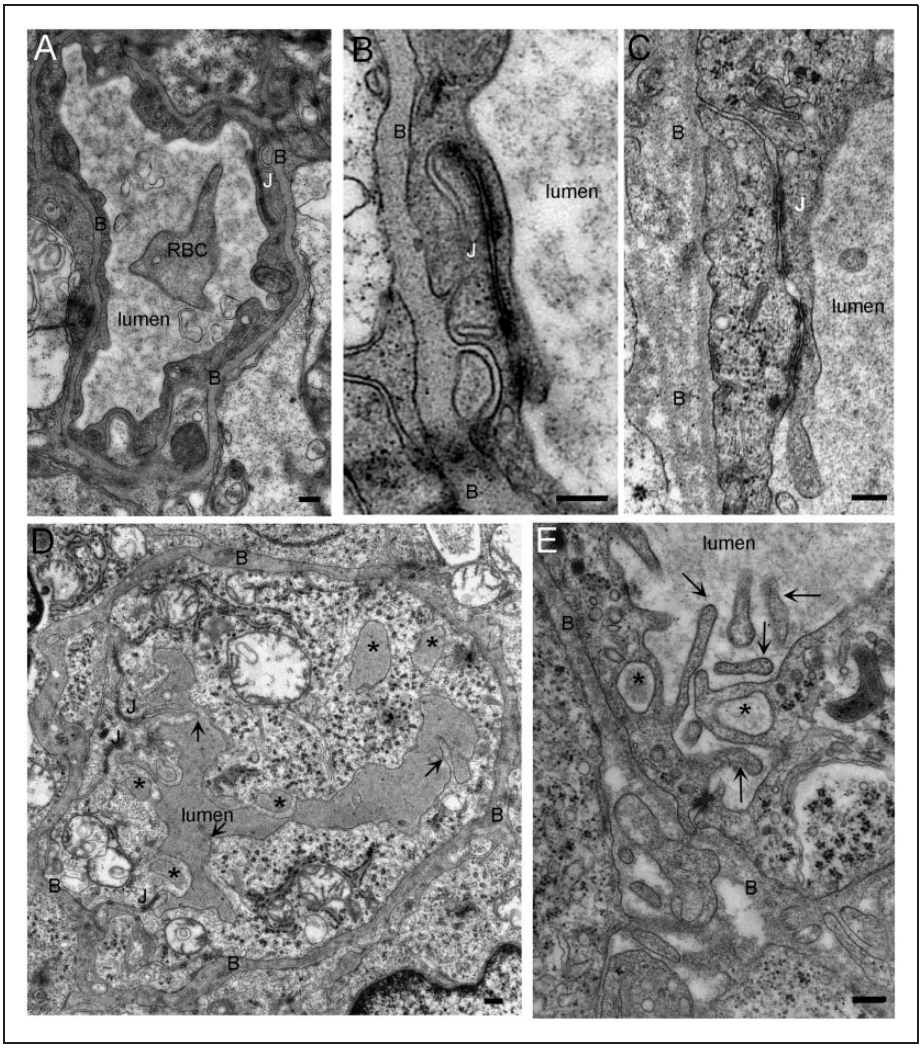

Figure 2. Morphology of the capillaries is modified in the tumor but tight junctions are still intact. (a) Transverse section of control capillary. The capillary wall is formed by thin endothelial cells that are connected by tight junctions (J). Surrounding the capillary is a basal lamina (B) beyond which is a covering of astrocytic processes. (b, c) Junctions between endothelial cells in control (b) and tumor capillaries (c). No difference in the length or the morphology is observed between the tight junctions of control and tumor capillaries. (d) Tumor capillary. Several membrane ruffles protrude in the lumen of the capillaries and the shape as well as the structure of the basal lamina is irregular. There are numerous macropinosomes (*) inside the endothelial cell. The electron density of these compartments is similar to that of the capillary lumen. (e) Detail of an endothelial cell. Membrane protrusions in the capillary lumen form cup shape profile that sometime fuse together to form macropinosome (*). Notice the disorganization of the basal lamina (c, d, and e). RBC: red blood cell (bar: 200 nm).

number of membrane protrusions in the capillary lumens (Figure 2(d) and (e), arrows). In the EM images, these protrusions appeared sometimes linked to the endothelial cells and sometimes as free tubular components due to cross section effects. These 120–150 nm long lamellipodia were devoid of ribosomes and seemed to contain actin microfilaments. To quantify the density of these protrusions, the number of lamellipodia in a capillary was divided by the inner circumference of that capillary. There were 3.29 ± 0.10 (94 capillaries obtained from three rats) and 1.07 ± 0.17 (141 capillaries obtained from three rats) lamellipodia in the lumen per 10 μm of endothelial cell membrane in the tumor and nontumor tissues, respectively ($p < 0.0001$). In the nontumoral tissue, protrusions were generally restricted to the TJ whereas in tumor tissue protrusions had no preferential location.

In the tumor, some of these protrusions showed a cup-shape profile, suggesting a fluid uptake mechanism by the endothelial cell. This uptake was further confirmed by the presence of large membrane compartments inside the endothelial cell (Figure 2(d) and (e), stars). The size of these compartments was above 200 nm, above that of endosomes. The electron density

inside these compartments was the same as that of the capillary lumen. Altogether, these observations suggest that these compartments result from the fusion of the lamellipodia in a macropinocytosis process.

Formation of lamellipodia in tumor endothelial cells is inhibited by amiloride

Macropinocytosis requires the remodeling of the actin cytoskeleton and is inhibited by amiloride, an inhibitor of the Na^+/H^+ exchanger that lowers the submembranous pH and prevents the association of the GTPases Rac1 and Cdc42 to the membrane.[15] Treatment with amiloride three days before analysis induced several modification of capillaries morphology including an accumulation of membrane components in the basal lamina, an enlargement of the endoplasmic reticulum of the endothelial cell and, in a few cases (~5%), an opening of junctions leading to continuities between the capillary lumen and the basal lamina (Figure 3(b) and (c), arrows).

In the lumen of these glioma capillaries, the number of lamellipodia protruding from endothelial cells dramatically decreased (Figure 3(a) and (e)), whereas membrane swelling and membrane blobs and vesicles were frequently observed in the lumen of the capillaries, suggesting defects in membrane remodeling and macropinocytosis process (Figure 3(a) and (d)). Such modifications were not observed in adjacent healthy tissues.

IgG diffuse from the lumen of tumor blood vessel to the extracellular space

Immunogold labeling showed that IgGs were highly concentrated in the lumen of all capillaries obtained in normal and tumoral tissues sampled from two rats. In healthy tissue, the IgG localization was restricted to the

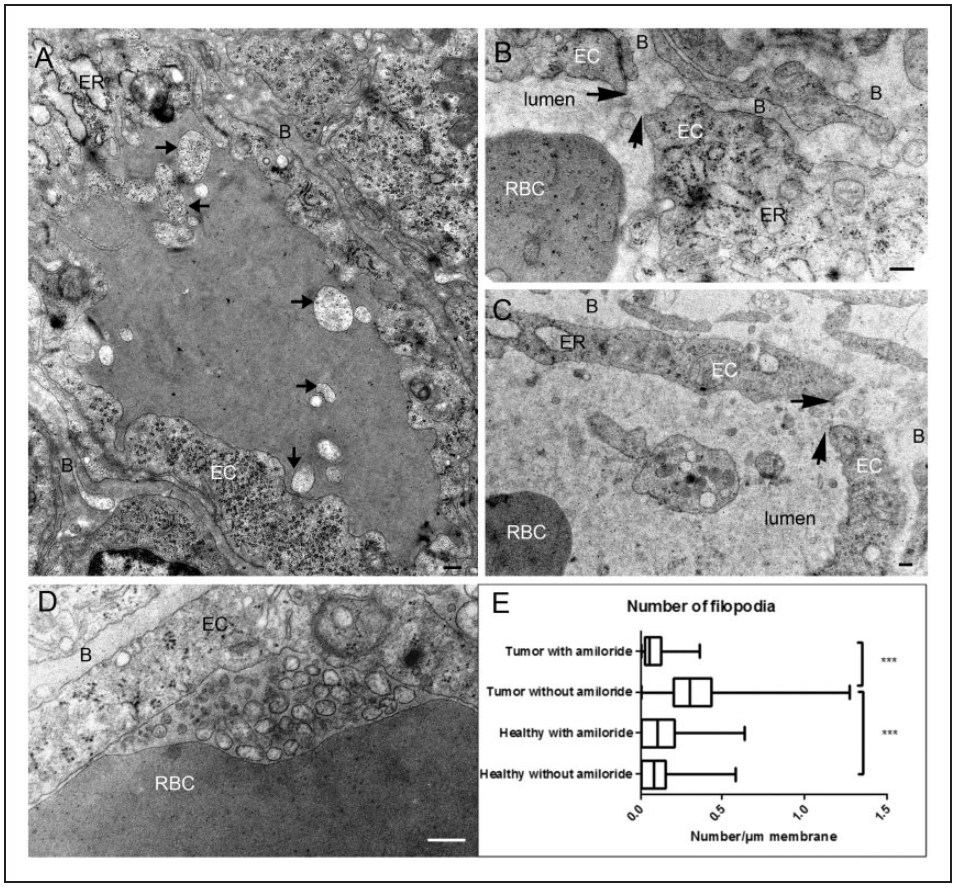

Figure 3. Tumor capillaries of amiloride-treated rats. (a) Cross section of a capillary. Dilatation of the endoplasmic reticulum (ER) could be observed in the endothelial cell, and heterogeneous membranes are present in the lumen of the capillary (arrows). (b, c) Opening of the junction (arrows) observed in amiloride-treated rats. Components of the blood diffuse in the basal lamina. (d) Accumulation of membranes vesicles in the lumen of the capillary. (e) Quantification of the number of protrusion in the lumen divided by the circumference of the capillary. Data are presented as boxplots with min/max values. B: basal lamina; EC: endothelial cell; ER: endoplasmic reticulum; RBC: red blood cell (bar: 200 nm).

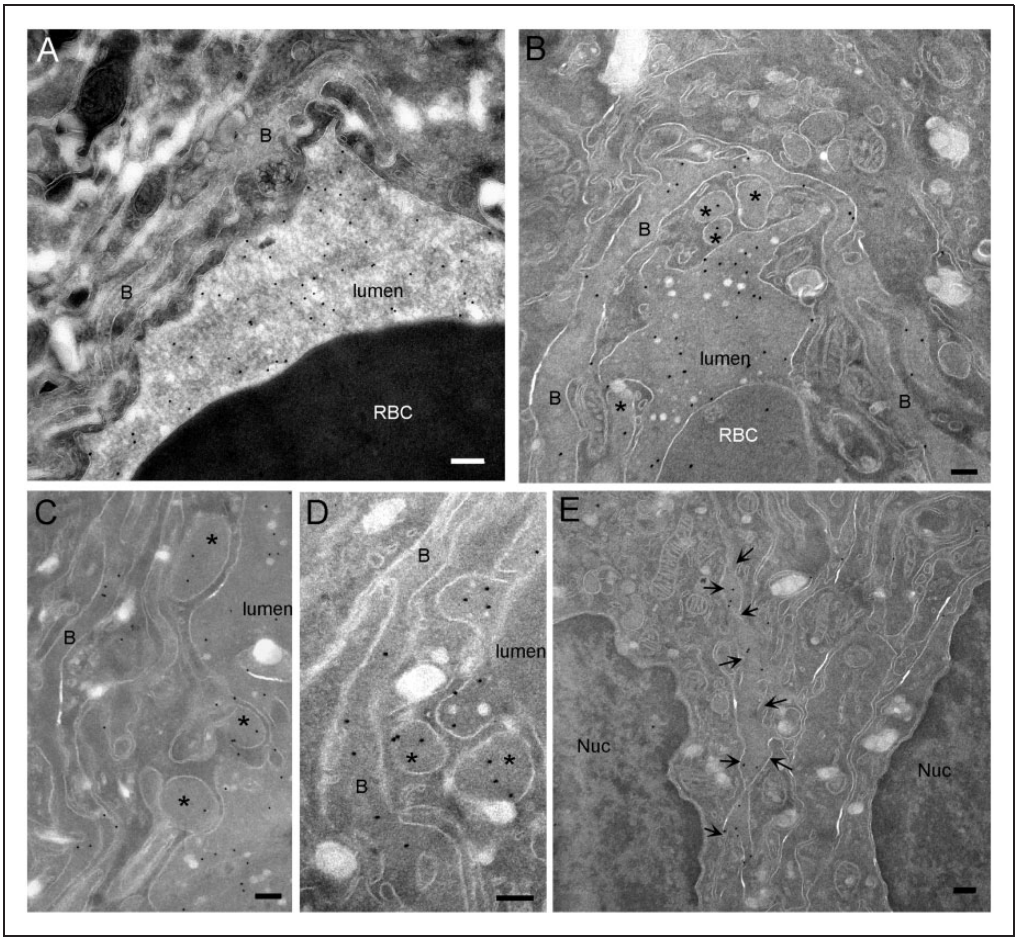

Figure 4. IgG diffuse from the lumen of tumor blood vessel to the extracellular space. (a) Control capillary. Protein A-gold labeling on cryosection shows that endogenous IgGs are located in the lumen of capillaries. Gold labeling is neither observed in the endothelial cells nor in the basal lamina. (b) In tumor, IgGs are located in the lumen of the capillaries, in the basal lamina and in macropinosomes (*). (c, d) In tumor, IgGs are located in macropinosomes inside the endothelial cell as well as in the basal lamina. Notice that IgG does not contact macropinosome membranes. (e) In tumor, protein A-gold labeling of IgG shows that endogenous antibodies diffuse between the tumor cells (arrows). B: basal lamina; Nuc: nucleus; RBC: red blood cell (bar: 200 nm).

lumen of the capillaries (16.60 ± 1.2 gold particles/μm^2) (Figure 4(a)) and only a few particles were detected in the basal lamina (0.38 ± 0.17 gold particles/μm^2). No particles were observed inside the endothelial cells or in the intercellular space. In the tumor tissue, a larger amount of IgG detected was localized in the basal lamina (7.4 ± 1.2 gold particles/μm^2; $p < 0.0001$ versus healthy tissue) (Figure 4(b) to (d)). Gold particles were also observed between tumor cells (Figure 4(e)) suggesting a transport of IgG from the capillary lumen to the tumor. Indeed, the high and homogenous density of IgG in the basal lamina and the tight sealing of endothelial junction do not support the hypothesis of a passage through the TJ but are in favor of an extravasation process through the endothelial cell. Because IgGs were not observed in clathrin-coated vesicles or in caveolae, our results suggest a nonclassical transcytosis mechanism of gold particles toward tumor tissue.

Indeed, our data are in agreement with a macropinocytosis uptake process for the following reasons: (i) the long protrusions observed in the capillary lumen sometimes formed cup shape profiles that engulfed the IgG. (ii) In the endothelial cells, IgGs were observed in membrane compartments larger than 200 nm (Figure 4(b) to (d), stars). IgGs were not particularly concentrated in the compartment, in line with a bulk transport process which does not involve the binding to a receptor. Since few macropinosomes were observed in each EM cross section, this suggests that the transport across the endothelial cell is either not frequent and/or occurs rapidly. The high density of IgG in the basal lamina indicates that IgGs are trapped in this matrix before diffusing in the intercellular space.

Permeability of the capillary is increased in the tumor

The anatomical T1w-MRI images obtained before and 100 min after USPIO injection showed that USPIO particles extravasate in RG2 glioma (Figure 5). A marked uptake of contrast agent was observed by MRI and was less pronounced in the center than in the periphery of the tumor. The quantification of the T1w-signal showed a $9.4 \pm 2.7\%$ increase in the tumor while a $8.3 \pm 4.3\%$ decrease was observed in the healthy tissue (striatum) in the absence of amiloride treatment ($n = 3$). After amiloride treatment ($n = 3$), the T1w-signal increased by $35.7 \pm 6.2\%$ in the tumor and decreased by $4.9 \pm 1.4\%$ in the control striatum, i.e. a reduction comparable to that in absence of amiloride. The signal decrease in the striatum may be ascribed to the presence of USPIO in the vessels which leads to a drastic reduction in the intravascular signal (T2 relaxivity effect) and to an additional reduction of the extravascular signal due to susceptibility effects. In the tumor, this effect is counterbalanced by the T1 effect that follows USPIO extravasation. Note that the tumor surfaces (measured in the MRI slice where the tumor appears the largest) were smaller in mice not treated with amiloride ($22.1 \pm 0.2\,mm^2$) than in those treated with amiloride ($30.1 \pm 3.4\,mm^2$). This difference in tumor size might explain in part the difference in permeability observed between the two groups. Nevertheless, these results show that amiloride does not prevent the extravasation of USPIO particles in the RG2 model and increases the MRI enhancement which becomes larger than in absence of amiloride, suggesting a different extravasation pathway.

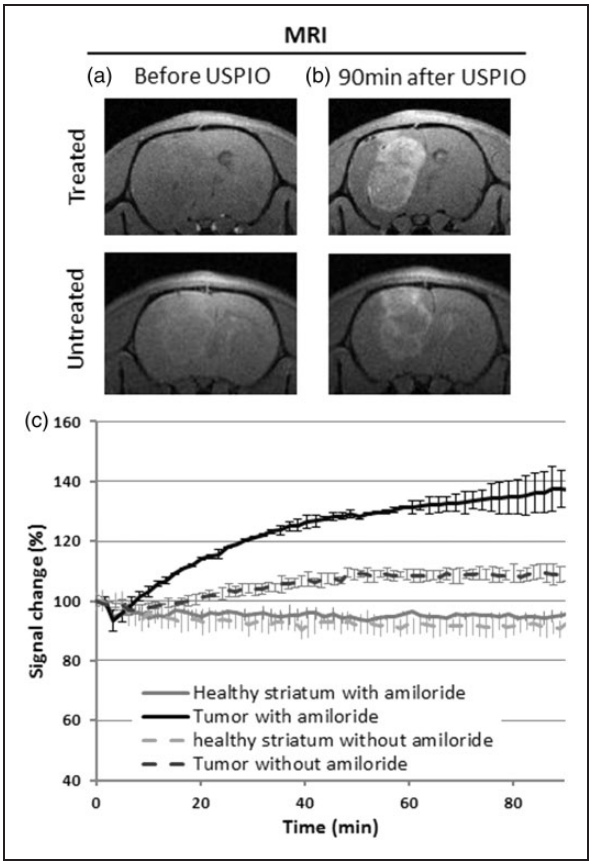

Figure 5. The extravasation of USPIO increases T1w signal in tumors. (a, b) T1w images obtained using MRI before and 90 min after injection of USPIO contrast agent in two rats bearing a RG2 glioma, one treated with amiloride and one not treated. After injection, the signal from the tumor rim is clearly enhanced with respect to the contralateral tissue. (c) Time course of the signal change obtained in two regions of interest (tumor and healthy striatum) and for the two groups of animals (with ($n = 2$) and without ($n = 2$) amiloride treatment). The signal of the first time point of each region of interest has been normalized to 100. Error bars stand for standard deviation. USPIO: ultrasmall superparamagnetic iron oxide.

Iron nanoparticles are also transported in macropinosomes

Using STEM for tumor analysis, electron dense particles were detected in the capillary lumen and in large membrane compartments inside the endothelial cells. The size of the iron oxide cores of the USPIO particles was heterogeneous and ranged from 2 to 10 nm. These cores were not uniformly round and the USPIO particles sometimes formed aggregates (Figure 6(a)).

The spectral analysis obtained by EDX confirmed that the particles contained iron (Figure 6(a) to (c), spectrum no. 1, 2, and 4), an element which was not detected in the red blood cell (Figure 6(b), spectrum no. 3). USPIOs were however not observed in the cytoplasm of endothelial cells or in transport vesicles like clathrin-coated vesicles or caveolae, suggesting that the transport of USPIO does not occur through a classical transcytosis mechanism. In addition, USPIOs were localized in 200 nm large compartments (Figure 6(b) and (c)). These two features match the observations made for IgG and suggest that USPIOs are transported via a macropinocytosis process.

Discussion

The purpose of this study was to identify specific abnormalities of the BTB in a RG2 glioma model. From a morphological point of view, the RG2 endothelial cells exhibited normal TJs but the basal lamina was enlarged and many lamellipodia protruded in the vessel lumen. From a functional point of view, the RG2 BTB allowed the extravasation of IgG and iron oxide particles, as observed by EM and MRI. Altogether, these results suggest that the extravasation of nanoparticles in

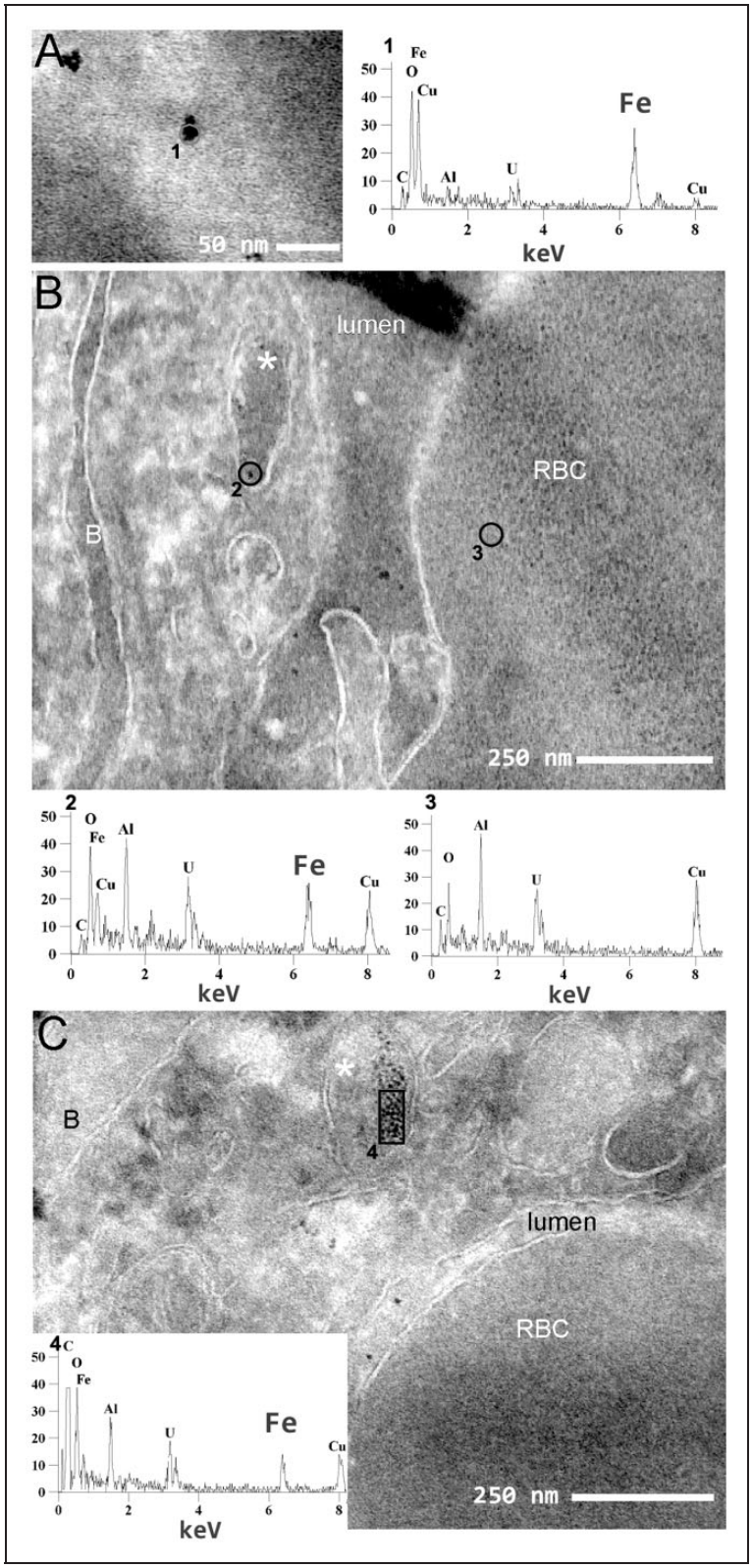

Figure 6. Iron nanoparticles are transported in large membrane compartment. Visualization of USPIO nanoparticles in the tumor using transmission scanning electron microscopy. (a) High magnification of USPIO nanoparticles in the lumen of a capillary (bar: 50 nm) and the chemical characterization of the particle by EDX (number of hits versus electron energy). The Kα peak of iron (Fe, 6.38 keV) is clearly visible. (b, c) Transverse sections of a capillary. Iron nanoparticles are visible in the capillary lumen as well as in a macropinosome (*). The chemical characterization by EDX confirms the presence of iron in macropinosomes whereas iron was not detected in the red blood cell (RBC). B: basal lamina; EDX: energy-dispersive X-ray; USPIO: ultrasmall superparamagnetic iron oxide (bar: 250 nm).

the RG2 model is an active process mediated by macropinocytosis rather than passive diffusion.

Our data demonstrate that open TJs were never observed in the RG2 glioma (more than 100 observations in three animals). Given the previously reported homogeneity of RG2 glioma at the growth stage used in this study,[14,19] and given that several samples were observed per animal, our data suggest that TJs are sealed throughout the entire RG2 tumor 15 days after implantation of 5×10^3 cells. This result was not expected as RG2 model is a mouse model whose vascular permeability for Gd-chelate (~1 nm in diameter) is well known and easily assessed by dynamic MRI.[14] The TJs are characterized by a high electron density at the membrane between the two endothelial cell parts. No significant difference was found between TJ from tumor and control tissue as the space between two endothelial cells was below 6 nm (5.8 ± 0.3 nm, 33 TJ from three rats), preventing the extravasation of IgG (~11 nm wide macromolecule[20]) and USPIO (~10–30 nm wide nanoparticle[17]). It can be assumed that TJs within the tumor tissue were opened very sparsely but this hypothesis is not in agreement with our observations showing a uniform distribution of IgG within the basal lamina.

It was previously reported[11] that TJ might be open in other tumor models but no recent reports on this subject were found in literature. From a methodological point of view, one has to be aware that a too high perfusion pressure during tissue fixation may cause a TJ opening. In this study, care was taken to fix the sample by immersion.

Several other mechanisms may be foreseen to explain how IgG and USPIO cross the endothelial cells in the RG2 glioma. Our work does not support the idea of an upregulation of regular transcytosis across the endothelial cell as very few vesicles were observed in the cytoplasm. Moreover, neither USPIOs nor IgGs were observed in such compartment. The formation of vesiculo-vacuolar organelles that cross endothelial cells has also been proposed as a possible extravasation pathway.[13] This assumption is however not compatible with the homogeneous distribution of IgG observed in the basal lamina. We are however aware that 2D EM is not the most appropriate approach to detect these 3D structures.

Nanoparticles and IgG were sometimes observed in large membrane compartments within the endothelial cells. The size of these compartments was above 200 nm, a value larger than the size of endosomes, compatible with a phagocytotic compartment. However, the absence of contact in our data between the limiting membrane and the cargo suggests that the observed uptake is nonspecific and thus does not support a phagocytosis hypothesis.[21,22] The electron density inside these compartments was the same as that of the capillary lumen, indicating that they resulted from a macropinocytotic uptake of intravascular fluid. Macropinocytosis is indeed known to be a constitutive form of endocytosis responsible for the fluid-phase uptake for several cell types such as macrophages and dendritic cells.[23] Macropinocytosis is based on actin-dependent reorganizations of the plasma membrane which form lamellipodia. Two protrusions—with a characteristic cup-shape profile—may eventually fuse to form a macropinosome, a morphologically heterogeneous vesicle without coat structure.[22] The characteristic cup-shape profiles and large compartments without coat structures were both observed within the tumor endothelial cells, in line with a nonspecific entrance of nanoparticules in tumor endothelial cells via macropinocytosis.

The macropinocytosis inhibitor amiloride is an orally administered diuretic that has been used clinically for more than three decades. It also indirectly inhibits macropinocytosis via a reduction in the submembranous pH.[15] In this study, amiloride clearly prevented the formation of the thin lamellipodia observed in the tumor endothelial cells, confirming that these protrusions were related to the macropinocytosis process. However, amiloride had other effects that dramatically modify the morphology of these capillaries; the most obvious of them was the opening of some TJ (~5%). Interestingly, the BTB permeability of RG2 glioma to iron oxide particles is increased following the opening of the TJ caused by amiloride, as observed by MRI. Amiloride is already used as an anticancer therapy[24] but our observations suggest another use of amiloride against cancer: it could serve to enhance the delivery of chemotherapy to glioma.

The exit of USPIO or IgG from the tumor endothelial cells requires a transcytotic transport of these macropinosomes. Such transport has previously been described in intestinal epithelial cells.[25] In our data, IgGs were mostly observed in the basal lamina, which was thicker and extended toward the intercellular space in this RG2 glioma. This represents an additional barrier to the diffusion of vascular nanomolecules.[26] This diffusion barrier would be less pronounced for a clinical Gd-chelate, thanks to its small hydrodynamic size (~1 nm). Extravasation of Gd-chelates in that RG2 glioma was previously observed by MRI.[14]

So far, macropinocytosis has not been reported as a constitutive characteristic of endothelial cells. However, it is well known that macropinocytosis can be induced by growth factors like the epidermal growth factor (EGF)[27] or the platelet-derived growth factor (PDGF).[28] Glioma such as RG2 secrete high levels of PDGF[29] and/or VEGF,[19,30] a cytokine originally described as vascular permeability factor due to its

ability to increase microvascular permeability to plasma proteins.[31] One could thus assume that, in some gliomas, macropinocytosis is induced in endothelial cells by a high level of growth factors secreted by the tumor cells. The existence of macropinocytosis in glioma is further supported by the analysis of clinical samples. Indeed, the presence of membrane protrusions in the luminal and abluminal membranes of the tumor endothelial cells has been reported as well as an increased density of membrane compartments within these cells.[10] Our data highlight that TJ opening yields a larger extravasation of iron oxide particles. In healthy endothelial cells, macropinocytosis appears as a natural adaptation of the cell to increase its transport rate. Conversely, TJ opening appears as a disruption of the BTB integrity. It would be of interest to further evaluate the relative contribution of macropinocytosis among the known BTB transport mechanisms.

Our observations suggest that the reduction in BTB permeability upon Bevacizumab treatment which prevents VEGF binding to its receptor[1] could be mediated by a reduction of the VEGF-induced macropinocytosis. In this case, antiangiogenic drugs would thus limit the nonspecific transport that occurs between blood and the tumoral tissue. It would be of interest to inspect other glioma models and patient tumor samples to evaluate whether macropinocytosis depends on the tumor subtype. This may be challenging in human samples given the known heterogeneity of glioma.

Altogether, these results indicate that drug delivery to glioma can occur via an active transport (macropinocytosis) rather than by a passive diffusion.

Funding

The author(s) disclosed receipt of the following financial support for the research, authorship, and/or publication of this article: This work received financial support from INSERM and University Joseph Fourier—Grenoble 1. IRMaGe was partly funded by the French program ''Investissement d'Avenir'' run by the ''Agence Nationale pour la Recherche''; grant ''Infrastructure d'avenir en Biologie Santé''—ANR-11-INBS-0006.

Acknowledgments

The authors thank Pascale Bayle Guillemaud for providing excellent working condition on the nanocharacterization facility of Minatec (CEA, Grenoble) and Claire Rome for her help in the amiloride experiment. The authors also acknowledge excellent help from the electron microscopy Facility, the MRI facility of Grenoble (IRMaGe), and the animal facility of the Grenoble Institute of Neurosciences.

Declaration of conflicting interests

The author(s) declared no potential conflicts of interest with respect to the research, authorship, and/or publication of this article.

Authors' contributions

Conception and design: KP-G, ELB
Development of methodology: KP-G, PHJ, ELB
Acquisition of data (provided animals, acquired and managed patients, provided facilities, etc.): RF, KP-G, PHJ, AB, JD
Analysis and interpretation of data (e.g. statistical analysis, biostatistics, computational analysis): KP-G, CR, ELB
Writing, review, and/or revision of the manuscript: ELB, KP-G, CR
Study supervision: ELB
Contributing tools: PHJ, KP-G, CR

References

1. Thompson EM, Frenkel EP and Neuwelt EA. The paradoxical effect of bevacizumab in the therapy of malignant gliomas. *Neurology* 2011; 76: 87–93.
2. Lemasson B, Serduc R, Maisin C, et al. Monitoring blood-brain barrier status in a rat model of glioma receiving therapy: dual injection of low-molecular-weight and macromolecular MR contrast media. *Radiology* 2010; 257: 342–352.
3. Abbott NJ, Ronnback L and Hansson E. Astrocyte-endothelial interactions at the blood-brain barrier. *Nat Rev Neurosci* 2006; 7: 41–53.
4. Liu X, Testa B and Fahr A. Lipophilicity and its relationship with passive drug permeation. *Pharm Res* 2011; 28: 962–977.
5. Plate KH, Breier G, Weich HA, et al. Vascular endothelial growth factor is a potential tumour angiogenesis factor in human gliomas in vivo. *Nature* 1992; 359: 845–848.
6. Dvorak HF. Vascular permeability factor/vascular endothelial growth factor: a critical cytokine in tumor angiogenesis and a potential target for diagnosis and therapy. *J Clin Oncol* 2002; 20: 4368–4380.
7. Connolly DT, Heuvelman DM, Nelson R, et al. Tumor vascular permeability factor stimulates endothelial cell growth and angiogenesis. *J Clin Invest* 1989; 84: 1470–1478.
8. Huber JD, Egleton RD and Davis TP. Molecular physiology and pathophysiology of tight junctions in the blood-brain barrier. *Trends Neurosci* 2001; 24: 719–725.
9. Tuma P and Hubbard AL. Transcytosis: crossing cellular barriers. *Physiol Rev* 2003; 83: 871–932.
10. Liebner S, Fischmann A, Rascher G, et al. Claudin-1 and claudin-5 expression and tight junction morphology are altered in blood vessels of human glioblastoma multiforme. *Acta Neuropathol* 2000; 100: 323–331.
11. Stewart PA, Hayakawa K, Hayakawa E, et al. A quantitative study of blood-brain barrier permeability ultrastructure in a new rat glioma model. *Acta Neuropathol* 1985; 67: 96–102.
12. Black KL and Ningaraj NS. Modulation of brain tumor capillaries for enhanced drug delivery selectively to brain tumor. *Cancer Control* 2004; 11: 165–173.
13. Feng D, Nagy JA, Hipp J, et al. Vesiculo-vacuolar organelles and the regulation of venule permeability to

macromolecules by vascular permeability factor, histamine, and serotonin. *J Exp Med* 1996; 183: 1981–1986.
14. Beaumont M, Lemasson B, Farion R, et al. Characterization of tumor angiogenesis in rat brain using iron-based vessel size index MRI in combination with gadolinium-based dynamic contrast-enhanced MRI. *J Cereb Blood Flow Metab* 2009; 29: 1714–1726.
15. Koivusalo M, Welch C, Hayashi H, et al. Amiloride inhibits macropinocytosis by lowering submembranous pH and preventing Rac1 and Cdc42 signaling. *J Cell Biol* 2010; 188: 547–563.
16. Kilkenny C, Browne W, National Centre for the Replacement R, et al. Animal research: reporting in vivo experiments—the ARRIVE guidelines. *J Cereb Blood Flow Metab* 2011; 31: 991–993.
17. Jung CW and Jacobs P. Physical and chemical properties of superparamagnetic iron oxide MR contrast agents: ferumoxides, ferumoxtran, ferumoxsil. *Magn Reson Imaging* 1995; 13: 661–674.
18. Slot JW and Geuze HJ. Cryosectioning and immunolabeling. *Nat Protoc* 2007; 2: 2480–2491.
19. Valable S, Lemasson B, Farion R, et al. Assessment of blood volume, vessel size, and the expression of angiogenic factors in two rat glioma models: a longitudinal in vivo and ex vivo study. *NMR Biomed* 2008; 21: 1043–1056.
20. Armstrong JK, Wenby RB, Meiselman HJ, et al. The hydrodynamic radii of macromolecules and their effect on red blood cell aggregation. *Biophys J* 2004; 87: 4259–4270.
21. Kerr MC and Teasdale RD. Defining macropinocytosis. *Traffic* 2009; 10: 364–371.
22. Swanson JA. Shaping cups into phagosomes and macropinosomes. *Nat Rev Mol Cell Biol* 2008; 9: 639–649.
23. Sallusto F, Cella M, Danieli C, et al. Dendritic cells use macropinocytosis and the mannose receptor to concentrate macromolecules in the major histocompatibility complex class II compartment: downregulation by cytokines and bacterial products. *J Exp Med* 1995; 182: 389–400.
24. Matthews H, Ranson M and Kelso MJ. Anti-tumour/metastasis effects of the potassium-sparing diuretic amiloride: an orally active anti-cancer drug waiting for its call-of-duty? *Int J Cancer* 2011; 129: 2051–2061.
25. Lukyanenko V, Malyukova I, Hubbard A, et al. Enterohemorrhagic *Escherichia coli* infection stimulates Shiga toxin 1 macropinocytosis and transcytosis across intestinal epithelial cells. *Am J Physiol Cell Physiol* 2011; 301: C1140–C1149.
26. Lieleg O, Baumgartel RM and Bausch AR. Selective filtering of particles by the extracellular matrix: an electrostatic bandpass. *Biophys J* 2009; 97: 1569–1577.
27. Haigler HT, McKanna JA and Cohen S. Rapid stimulation of pinocytosis in human carcinoma cells A-431 by epidermal growth factor. *J Cell Biol* 1979; 83: 82–90.
28. Davies PF and Ross R. Mediation of pinocytosis in cultured arterial smooth muscle and endothelial cells by platelet-derived growth factor. *J Cell Biol* 1978; 79: 663–671.
29. Sibenaller ZA, Etame AB, Ali MM, et al. Genetic characterization of commonly used glioma cell lines in the rat animal model system. *Neurosurg Focus* 2005; 19: E1.
30. Goldman CK, Kim J, Wong WL, et al. Epidermal growth factor stimulates vascular endothelial growth factor production by human malignant glioma cells: a model of glioblastoma multiforme pathophysiology. *Mol Biology Cell* 1993; 4: 121–133.
31. Bates DO, Hillman NJ, Williams B, et al. Regulation of microvascular permeability by vascular endothelial growth factors. *J Anat* 2002; 200: 581–597.